Natural history study and statistical modelling of disease progression in a preclinical model of myotubular myopathy

Suzie Buono[1*], Arnaud Monseur[2*], Alexia Menuet[1], Anne Robé[1], Catherine Koch[1], Jocelyn Laporte[3], Leen Thielemans[1,4], Marion Depla[1], Belinda S. Cowling[1]

[1]Dynacure, Illkirch, France
[2]Pharmalex, Mont-St-Guibert, Belgium
[3]IGBMC, Inserm U1258, CNRS UMR7104, Université de Strasbourg, Illkirch, France
[4]2Bridge, Zoersel, Belgium

*Equal contribution to this work
‡Correspondence may be addressed to B.S.C (belinda.cowling@dynacure.com); ORCID ID: 0000-0001-6915-2596

Key words: Centronuclear myopathies, Myotubular myopathy, Preclinical disease models, Dynamin, Antisense oligonucleotides, therapy, neuromuscular disorders

Summary Statement: This study optimized disease severity analysis and modelled disease progression in XLMTM mice, and confirmed this model using therapeutic *Dnm2* reduction in a dose-response study.

Abstract

Generating reliable preclinical data in animal models of disease is essential in therapy development. Here we perform statistical analysis and joint longitudinal-survival modelling of the progressive phenotype observed in *Mtm1*$^{-/y}$ knock-out mice, a faithful model for myotubular myopathy (XLMTM). Analysis of historical data was used to generate a model for phenotype progression, which was then confirmed with phenotypic data from a new colony of mice derived via in vitro fertilization in an independent animal house, highlighting the reproducibility of disease phenotype in *Mtm1*$^{-/y}$ mice. This combined data was then used to refine the phenotypic parameters analyzed in these mice, and improve the model generated for expected disease progression. The disease progression model was then used to test therapeutic efficacy of *Dnm2* targeting. *Dnm2* reduction by antisense oligonucleotides blocked or postponed disease development, and resulted in a significant dose-dependent improvement outside the expected disease progression in untreated *Mtm1*$^{-/y}$ mice. This provides an example of optimizing disease analysis and testing therapeutic efficacy in a preclinical model, that can be

applied by scientists testing therapeutic approaches using neuromuscular disease models in different laboratories.

Introduction

In a research setting, mouse models of disease provide an excellent tool to investigate disease pathophysiology and test therapeutic approaches. Mouse lines that recapitulate the disease phenotype can be used to identify novel therapeutic targets, and map in a temporal and dose-dependent manner the response to treatment. Animal models may also be useful in identifying and testing diagnostic, prognostic or therapeutic biomarkers. Pathological phenotypes in animals may be compared with the human disease, to help gain insight into the underlying pathophysiology that is relevant for patients, and to test the potential of various therapeutic modalities targeting the mechanism-of-action, including small molecules (chemically derived) and various biologics (eg. gene and cell therapies).

Many potential therapies for neuromuscular diseases have moved from proof-of-concept in animal studies towards clinical trials in the past decade (Cowling and Thielemans 2019). Often, proof-of-concept is generated using preclinical animal models of neuromuscular disease; however translating preclinical data to a clinical setting is often challenging. Mouse models of human disease have limitations, which may be linked to the relatively uniform genetic background of animal cohorts compared to humans and the potentially complex genetic involvement in inherited neuromuscular disorders (causative gene and epistatic mutations), and the targeting of pathogenic pathways which might not be similar between species. Considering these limitations is important when interpreting animal data. Optimizing the generation of relevant, reliable and reproducible preclinical data on disease phenotype and therapeutic potential is of high importance. Natural history studies in mice are a useful way to understand disease progression and standardize phenotyping parameters across studies. This has been performed in recent years in mdx mice; a frequently used mouse line to investigate Duchenne Muscular Dystrophy (van Putten et al. 2019; Gordish-Dressman et al. 2018).

In this study we focus on a preclinical animal model for myotubular myopathy. Myotubular myopathy is a non-dystrophic, debilitating rare congenital disease, associated with muscle weakness and abnormally located nuclei and other organelles in skeletal muscle (Ravenscroft, Laing, and Bonnemann 2015). Myotubular myopathy (also called X-linked CNM (centronuclear myopathy), XLCNM, XLMTM, OMIM 310400) is due to mutations in the phosphoinositides phosphatase myotubularin (MTM1) (Laporte et al. 1996). There are an estimated 2650 living patients with myotubular myopathy, in the US, EU, Japan and Australia (Vandersmissen et al. 2018) . *Mtm1*$^{-/y}$ mice recapitulate myotubular myopathy; as observed in patients, mice display a severe myopathic phenotype and a reduced lifespan (Buj-Bello et al. 2002). This model has been used across laboratories from several continents, and has been used to provide the therapeutic proof-of-concept and supportive data contributing to the rationale for initiating several clinical trials (NCT04915846, NCT03199469; NCT04033159), thus highlighting the importance of data generated from this model. Recent studies suggested increased DNM2 was largely responsible for the Centronuclear Myopathy phenotype observed in mice and patients (Cowling et al. 2014; Cowling et al. 2011; Liu et al. 2011; Massana Munoz et al. 2019). Reduction of DNM2 was shown to rescue myotubular myopathy in mice (*Mtm1*$^{-/y}$ mice) by genetic cross (Cowling et al. 2014), systemic delivery of

antisense oligonucleotides (Tasfaout et al. 2017; Koch et al. 2020), and by reducing DNM2 using an AAV-mediated shRNA approach targeting *Dnm2* (Tasfaout et al. 2018).

The goal of this study was to describe disease progression and the variability with which it can occur & to inform which phenotypic parameters are sufficient to predict disease progression in *Mtm1*$^{-/y}$ mice. We perform statistical analysis and modelling of the progressive phenotype observed in *Mtm1*$^{-/y}$ mice from retrospective ('training') and prospective ('test') data generated in *Mtm1*$^{-/y}$ mice. This combined data was then used to improve both the phenotyping analysis performed in these mice, and the model generated for normal disease progression. Finally this model was tested and validated by performing a therapeutic dose response study targeting *Dnm2*.

Results

Natural History Study analysis and model generation from training cohort

To generate a statistical model of disease progression in myotubular myopathy mice, we first focused on performing an analysis of previous natural history data generated from *Mtm1*$^{-/y}$ mice across several studies (Koch et al. 2020), referred to as the 'training cohort'. Analysis of 38 mice from weaning identified the normal survival curve for *Mtm1*$^{-/y}$ mice, with loss of survival starting from 3-4 weeks of age, and no mice surviving past 8 weeks of age (Figure 1A). Analysis of body weight progression in mice showed the average weight of 3 week old mice at the start of the study was 10.31±1.27g (mean±standard deviation, SD). In the majority of mice this increased from weeks 3-4, followed by a decline in body weight, with no mice reaching 20g in this study (Figure 1B). Next, a joint model was generated from the raw body weight data, considering both survival and evolution of body weight. Based on this model, the line of best fit and prediction intervals for the expected range of body weights for *Mtm1*$^{-/y}$ mice was modelled (Figure 1B: black line, grey shadow respectively).

Hanging time upside down from a cage lid with 4 paws, was used as an indicator of whole body strength in mice, and averaged approximately 50 seconds at 3 weeks of age in *Mtm1*$^{-/y}$ mice (Figure 1C). From 5 weeks of age almost no mice could perform the test for more than 5 seconds, compared to wildtype mice which can normally hang for the maximum time tested, 60 seconds, at all time points analyzed (Koch et al. 2020). As statistical modelling for prediction to perform the test in this format was not feasible, we performed a time to event analysis, selecting hanging time ability cut off times of 50 (Figure 1D) or 10 (Figure 1E) seconds. At 3 weeks of age approximately 60% of *Mtm1*$^{-/y}$ mice could hang for more than 50 seconds, whereas by 5 weeks of age almost no mice could perform this test more than 10 seconds (Figure 1D,E), indicating rapid and severe progression of the myopathic phenotype during this age bracket.

To capture key disease elements and monitor severity and progression of disease in *Mtm1*$^{-/y}$ mice, previously a disease severity score was created (Tasfaout et al. 2017)(Supplementary Table 1). The disease severity score (DSS) was designed to capture key phenotypic elements of myopathy phenotype apparent in mice. This focused primarily on 6 key factors; body weight, hanging test (whole body strength), kyphosis (curvature of the spine), walking ability (hind limb muscle weakness), ptosis (eyelid muscle weakness), and difficulties in breathing (Table 1). Disease severity score analysis was performed on training cohort data, and modelling was performed to identify the line of best fit and prediction

interval of expected scores (Figure 1F). Mice exhibited an average disease severity score of 0.88 ± 0.55 (mean±SD) at 3 weeks of age, which progressed to 4.44 ± 0.42 (mean±SD) by 8 weeks of age, suggestive of a severe disease phenotype in *Mtm1*$^{-/y}$ mice surviving until 8 weeks of age. Overall analysis of survival and phenotyping data from the training cohort confirm drastically reduced survival and a severe progressive myopathic phenotype in *Mtm1*$^{-/y}$ mice from weaning until 8 weeks of age.

Natural History Study in test cohort of myotubular myopathy mice

Following on from analysis of historical data in the training cohort, we next performed a natural history study in 20 *Mtm1*$^{-/y}$ mice after weaning, designated 'test cohort'. Of note this colony was generated by *in vitro* fertilization (IVF) from samples taken from *Mtm1*$^{-/y}$ mice from the colony used to generate the training cohort. IVF and colony generation was performed in a separate animal housing facility at a different location, thus more accurately representing the comparison of preclinical research experiments by multiple research laboratories in different locations.

Analysis of survival in the test cohort of *Mtm1*$^{-/y}$ mice was performed. Loss of survival was observed from 3-4 weeks of age, and no mice survived past 12 weeks of age (Figure 2A), suggesting more variation in survival in the test cohort compared to the training cohort (Figure 1A). Based on the body weight data generated in the training cohort (based on raw data up to 8 weeks of age), a model was generated to display the line of best fit (= median profile) and prediction interval expected for body weight progression in *Mtm1*$^{-/y}$ mice (Figure 1B). Body weight was then analyzed weekly in the test cohort, and overlaid on the model generated from training data, including extrapolation of expected prediction interval for 8-12 weeks of age. All mice fell within the expected weight range for *Mtm1*$^{-/y}$ mice over the period analyzed (3-12 weeks of age), confirming the reproducibility of body weight progression in this mice line (Figure 2B). Consistent with the training colony, no mice reached 20g body weight.

To analyze whole body strength, the hanging test was then performed in the test cohort of *Mtm1*$^{-/y}$ mice. As observed in the training cohort (Figure 1C), hanging time rapidly declined in mice from 3-5 weeks of age (Figure 2C). A statistical comparison between training and test cohorts was performed using a time to response analysis (Figure 2D,E), confirming the reliability of this test as an indicator of whole body strength in *Mtm1*$^{-/y}$ mice.

Finally, the combined disease severity score was analyzed. Based on the model generated from the training cohort (Figure 1F) which included extrapolation of expected prediction interval for 8-12 weeks of age, all mice fell within the expected disease severity score over the period analyzed (Figure 2F, 3-12 weeks of age), confirming the reproducibility and reliability of disease severity score progression in this mice line, and the analytical validity of the model generated.

Optimized Disease Severity analysis based on combined natural history study data from training and test cohorts

Based on the large volume of data generated above, we next aimed to optimize the disease severity analysis performed in *Mtm1*$^{-/y}$ mice, by focusing on a statistical modelling approach. Firstly combined analysis of the survival of *Mtm1*$^{-/y}$ mice highlighted that deaths can occur from the age of weaning at 21

days (youngest age analyzed in this study), until 12 weeks of age, with less than 50% of *Mtm1*$^{-/y}$ mice surviving past 5 weeks of age, compared to 100% of WT mice (Figure 3A).

Next we investigated the disease severity in the combined training and test cohorts. The disease severity score is comprised of 6 factors: body weight, hanging test, kyphosis, walking ability, ptosis, and difficulties breathing, as described in table 1. The progression of each of the individual 6 factors of the combined training and test mouse cohorts is shown in figure 3B (average values shown). Whilst body weight, hanging, walking and kyphosis reflected early disease progression in *Mtm1*$^{-/y}$ mice from 3-7 weeks of age, breathing and ptosis did not reflect disease progression, with elevated scores only occurring after 7 weeks of age when 20% of mice are still alive. Therefore we decided to focus on the four factors best reflecting early disease progression. Body weight progression in *Mtm1*$^{-/y}$ mice (Figure 3C, red) clearly identified a pattern of weight gain, not reaching a maximum of 20g, before a sharp decline in body weight prior to death, compared to wild type mice (black) which continued to increase in body weight. On average body weight decline started 2.3 weeks before death, with an average loss of 2.16±1.07g body weight. For this reason the parameters measuring body weight were optimized to reflect body weight gain (0, expected in healthy juvenile mice), stabilization (0.5), or decline (1) relative to the prior week in the same mouse (table 1), rather than relative to wildtype mice. Hanging test, reflecting whole body strength, was identified as the best representative of the myopathic phenotype in *Mtm1*$^{-/y}$ mice, with a rapid decline in performance identified from 3-5 weeks of age, compared to wild type mice which could perform the test for the duration of the experiment (Figure 3D). Consequently hanging ability was given a higher weight of 2 points. It was also constructed as a continuous score between 0 and 2 instead of the previously used categorical scores of 0, 0.5 and 1 (table 1, supplementary table 1). The scores for kyphosis and walking were deemed appropriate and no optimization was required. The line of best fit for each disease severity score parameter is shown in figure 3E, updated based on statistical analysis and modelling of natural history study data from training and test cohorts in mice, and reflecting a progressive and severe development of all disease phenotypes analyzed in *Mtm1*$^{-/y}$ mice from 3-12 weeks of age. Of note the 2 functional tests were the first to decline in *Mtm1*$^{-/y}$ mice; hanging ability (whole body strength) and walking ability, followed by a decline in physical parameters; kyphosis and finally body weight.

The next step was to combine these factors for an overall disease severity score, with a maximum value of 5. Individual progression of the optimized disease severity score is shown for *Mtm1*$^{-/y}$ mice, confirming a rapid disease progression from 3 weeks of age (Figure 3F). This data was then used to optimize the disease severity score model, represented on the graph with the line of best fit and prediction interval shown (Figure 3F). Not surprisingly, all mice from training and test cohorts fell within the predicted range for almost all timepoints analyzed. A standard operating procedure (SOP) to perform this optimized disease severity score can be found in the supplementary information of this manuscript (Annex 1).

Investigation of post mortem muscle phenotypes in *Mtm1*$^{-/y}$ mice

We next wanted to assess if the disease severity phenotype observed in *Mtm1*$^{-/y}$ mice correlated with muscle pathology. To this end we examined the muscle mass of several skeletal muscles. Muscle atrophy was similarly observed across TA, gastrocnemius and quadriceps skeletal muscles (2-3 fold reduction in mass, Figure 4A; 1.5-1.9 fold relative to body weight, Supplementary Figure 1A,B). Muscle

mass correlated with disease severity in *Mtm1*$^{-/y}$ mice from all skeletal muscles analyzed (Figure 4B-D). As the name suggests 'centronuclear myopathy' results in the abnormal positioning of nuclei internally within muscle fibers. Focusing on the TA muscle, fiber diameter and nuclei position was significantly altered in *Mtm1*$^{-/y}$ mice versus wildtype mice (Figure 4E-I). Although a significant correlation was observed when analyzing disease severity score compared to fiber size and nuclei position in wild type and *Mtm1*$^{-/y}$ mice, no correlation was observed when analyzing only *Mtm1*$^{-/y}$ mice at 5 weeks of age (Figure 4H,J). This may be explained by the muscle function parameters of the DSS (walking and hanging ability) which are already nearly maximally affected by this age, whereas the variable component at this age (kyphosis and body weight) are less related to muscle structure and function (Figure 3E).

Validation of the model in a dose response study following DNM2 reduction

The final step to validate the disease severity model generated was to test a therapeutic intervention in *Mtm1*$^{-/y}$ mice. Reduction of DNM2 by systemic delivery of antisense oligonucleotides was shown to rescue myotubular myopathy in 3-week old *Mtm1*$^{-/y}$ mice in a dose-response manner (Tasfaout et al. 2017; Koch et al. 2020). Here we tested the dose-response effect of treatment of *Mtm1*$^{-/y}$ mice with antisense oligonucleotides targeting murine *Dnm2*, by weekly intraperitoneal dosing from 5 weeks of age, an age where mice are already severely affected by the disease (Figure 3). Three doses were selected; low, mid, and high (6.25, 12.5, 25mg/kg respectively) doses of DYN101-m targeting murine *Dnm2* or ASO control (25mg/kg) (Tasfaout et al. 2017), and were delivered weekly by intraperitoneal injection from 5 to 12 weeks of age. A clear increase in survival was observed in *Mtm1*$^{-/y}$ mice at all doses tested (Figure 5A), compared to untreated *Mtm1*$^{-/y}$ mice in this study. All wild type mice survived for the duration of this study. As no dose-response was identified in survival in this study, survival data across groups was then combined and compared to untreated *Mtm1*$^{-/y}$ mice. Combined survival analysis, represented as mean±95% confidence interval (Figure 5B), was clearly above the survival observed in untreated *Mtm1*$^{-/y}$ mice, indicating that survival significantly increased following DYN101-m administration in this trial.

To investigate the therapeutic effect of DNM2 reduction on disease severity in *Mtm1*$^{-/y}$ mice, we next analyzed each of the four disease severity score parameters in mice from the dose response study. Regarding physical parameters; body weight progression (Figure 5C) and kyphosis (Figure 5D), a clear improvement was observed in *Mtm1*$^{-/y}$ mice following reduction of DNM2 at all doses at the completion of the study (12 weeks of age). Of note *Mtm1*$^{-/y}$ mice injected with the low dose (6.25mg/kg) showed a delayed response for improvement compared to mid and high doses (12.5 and 15mg/kg respectively), in presentation of kyphosis. A clear improvement was observed in functional parameters; walking (Figure 5E) and hanging ability (Figure 5F), at mid and high doses, whereas no improvement was observed in these parameters at low dose, despite the improved survival. Furthermore a delayed improvement in hanging test ability was observed in mid-dose compared to high-dose, suggesting a dose-response effect.

Finally, the combined disease severity score was analyzed in *Mtm1*$^{-/y}$ mice treated with antisense oligonucleotides targeting *Dnm2*. An improvement in disease severity score was observed in all dose ranges tested (Figure 5G), with all doses resulting in mice with reduced disease severity scores, outside of the predicted range for untreated *Mtm1*$^{-/y}$ mice of the same age (Figure 5H). Importantly, a dose-response effect was observed, with higher doses resulting in a more rapid improvement of the disease

phenotype, thus validating the disease severity model generated, and confirming a reduction of the myopathy features in a dose response manner, following *Dnm2* reduction.

Histopathological analysis of dose response study with DNM2 therapy

To support the improvement in survival and myopathic phenotype observed following ASO delivery to *Mtm1*$^{-/y}$ mice, we next investigated post-mortem skeletal muscle specimens at the molecular level at 12 weeks of age. Comparison of treated *Mtm1*$^{-/y}$ mice was only possible with wild type mice, as untreated *Mtm1*$^{-/y}$ mice do not survive until this age. Following weekly intraperitoneal administration of ASO targeting *Dnm2* into mice, a significant dose-dependent reduction of *Dnm2* mRNA was observed (39-69% reduction, Figure 6A). Skeletal muscle mass was increased when analyzed alone or relative to body weight in a dose response in both gastrocnemius and TA skeletal muscles (Supplementary Figure 1C-F), which correlated with the reduction in disease severity score observed (Figure 6B, Figure 5G, Supplementary Figure 1G).

We next investigated if the reduced myopathic phenotype observed following *Dnm2* reduction correlated with an amelioration of the structural defects observed in *Mtm1*$^{-/y}$ mice. Corresponding to the improved whole body strength observed following *Dnm2* reduction (Figure 5), an improvement in fiber size was also observed, with no statistical difference observed in the top dose tested compared to wild type control mice (Figure 6C,D). Furthermore this correlated with the improvement in disease severity score (Figure 6E). Whilst mice with the lowest dose still presented with 20.5±3.2% of centralized nuclei, consistent with previously published data in *Mtm1*$^{-/y}$ mice versus 0-2% in WT mice (Tasfaout et al. 2017; Koch et al. 2020), this was reduced to 9.4±4.6% in the high dose group, suggesting a dose-dependent improvement in nuclei position in our study (Figure 6D,F). This was further supported by a clear amelioration of the abnormal organelle accumulations observed by succinate dehydrogenase staining of skeletal muscles (Figure 6D). Importantly, a significant correlation was observed between the disease severity score (DSS) and nuclei position across mice and across doses (Figure 6G). Of note, whilst an improvement in survival and disease severity was observed in low dose mice at 12 weeks of age outside of the modelled expected values of *Mtm1*$^{-/y}$ mice at 12 weeks of age (Figure 5A,G), these mice displayed similar results to untreated *Mtm1*$^{-/y}$ mice at 5 weeks of age (Figure 6B,E,G red overlay). Therefore antisense oligonucleotide mediated reduction of *Dnm2* resulted in a significant dose-dependent improvement in disease phenotype, with a clear improvement outside the expected disease progression in untreated *Mtm1*$^{-/y}$ mice.

Discussion

The purpose of this study was to (1) validate statistically the disease phenotype in *Mtm1*$^{-/y}$ mice; and (2) use this data to generate the first joint longitudinal-survival model of disease progression in this mouse line, which is highly relevant for testing therapeutic approaches preclinically in mice. This study provides an example of optimizing analysis of disease progression and testing therapeutic efficacy in a preclinical model of myotubular myopathy.

Modelling disease progression in *Mtm1*$^{-/y}$ mice. In this study we performed disease progression modelling, to provide an optimized model of disease progression in *Mtm1*$^{-/y}$ mice over time based on natural history survival and phenotyping data. The consistency of the disease phenotype between mice from the same colony, and between colonies is important to understand preclinical disease models. Variability may occur in the phenotype between mice in the same colony, that may affect interpretation of the data generated. Here we observed minor differences in survival between colonies, which were factored into the survival probability curve generated (Figure 3A). Survival rates observed in training and test cohorts were consistent with recently published data from the same mouse line housed in three different laboratories (Maani et al. 2018; Gayi et al. 2018; Daniele et al. 2018). Furthermore both body weight progression and overall disease severity parameters were consistent between colonies (Figure 2B-F), and used to optimize the model generated for disease severity mapping in *Mtm1*$^{-/y}$ mice (Figure 3). Of interest – muscle mass correlated with disease severity parameters in 5 week old *Mtm1*$^{-/y}$ mice, however no correlation was observed between overall disease severity and muscle histology analysis (Figure 4), suggesting muscle histopathology does not reflect the full disease spectrum in this model.

Understanding the natural history of the disease model is the first step, which is required to determine study parameters for testing a therapeutic approach, such as timing of the intervention and appropriate parameters to test for therapeutic effects. Here the data generated was used to select the relevant parameters to analyze disease progression in *Mtm1*$^{-/y}$ mice, and improve the disease severity scoring system using statistically powered data. The model developed here from phenotyping of over 50 *Mtm1*$^{-/y}$ mice from two independent colonies suggests a progressive myopathic phenotype in mice, which provides a window for testing therapeutic potential post weaning (Figure 3). This statistical model will be made available to any researcher working with this mouse line, which can be of use to validate future therapeutic approaches tested on this mouse line in different laboratories. One strength of this approach is the data used to generate this model came from two independent colonies housed in independent breeding facilities, thus more faithfully representing variation observed by different research laboratories. This modelling approach suggests a method to validate preclinical phenotyping data and therapeutic efficacy, that may be applied by scientists testing therapeutic approaches using other neuromuscular disease models. Sharing of historical phenotyping data and modelling approaches across publicly accessible platforms is an important collaborative step that researchers can contribute to, which can help to increase the reliability of preclinical data generated.

Use of preclinical models to test therapeutic efficacy. It is of high importance to statistically validate both the model(s) used for neuromuscular disorders, and analyze therapeutic efficacy in an unbiased manner. We used the model generated here of disease progression in *Mtm1*$^{-/y}$ mice, to validate if reducing *Dnm2* expression improves survival and disease phenotype in these mice. Targeting *Dnm2* by antisense oligonucleotide-mediated reduction blocked disease progression (low dose) and resulted in a significant reduction in disease phenotype (mid/high dose), with a clear improvement outside the normal range of disease progression in *Mtm1*$^{-/y}$ mice in all dose groups (Figure 5). This study followed on from the initial proof-of-concept study validating targeting *DNM2* with antisense oligonucleotides as a potential target for therapy (Tasfaout et al. 2017), and was carefully designed to test disease reversion in a dose-response study (Figures 5,6)(Koch et al. 2020).

Performing statistically powered blinded studies can help improve the correct interpretation of preclinical data, as can reproducing data from more than one colony. Initiatives such as the TREAT-NMD neuromuscular network offer support for preclinical research (https://treat-nmd.org/research-

overview/) and guidance and advice to scientists on the different aspects of translational research related to therapy development programs in neuromuscular disorders, with the aim of improving translational efficacy for the benefit of patients (Treat-NMD advisory committee (TACT))(Willmann et al. 2020). Therapeutic data in mouse models of disease often provides the main or sole data source supporting therapeutic improvement in disease presentation, with the majority of the supportive non-clinical data aimed at reducing any potential safety risk(s) to patients and understanding pharmacokinetics to translate the dose to the human context (Cowling and Thielemans 2019). Currently 3 clinical trials (NCT04915846 NCT03199469; NCT04033159, the latter supported by data generated here) have been initiated following therapeutic proof-of-concept observed from three independent therapeutic approaches in this mouse model (Buj-Bello et al. 2008; Buono et al. 2018; Tasfaout et al. 2017; Maani et al. 2018; Gayi et al. 2018). Of note preliminary therapeutic efficacy has been observed in myotubular myopathy patients following preliminary data generated with the most advanced of the therapeutic approaches (Shieh et al. 2020), supporting the potential utility of *Mtm1*$^{-/y}$ mice as a disease model for relevant myotubular myopathy disease phenotypes in patients.

In conclusion, we present here a statistical modelling approach of disease progression in myotubular myopathy mice, and validate the reliability of this model by testing a therapeutic approach in this mouse line in a dose-response study. This approach can be applied by researchers across the neuromuscular field, to support the generation of reliable and reproducible preclinical data. Using this approach may thus improve confidence in preclinical therapeutic data generated from neuromuscular disease models across different laboratories or across different cohorts.

Materials and methods

Generation of *Mtm1*$^{-/y}$ mice. *Mtm1*$^{-/y}$ or WT 129SvPAS mice were previously generated and characterized by crossing *Mtm1* heterozygous females obtained by homologous recombination with WT males (Buj-Bello et al. 2002). The training cohort was previously generated at the IGBMC (Illkirch, France), and historical published data generated from this cohort was obtained and analyzed from 3 weeks of age ((Koch et al. 2020) studies 3, 5, n=38 *Mtm1*$^{-/y}$ mice). To generate the test cohort, in vitro fertilization was performed at Janvier Labs in the 129SvPAS strain (Saint-Berthevin, France), then offspring were transferred to Chronobiotron (Strasbourg, France) for colony generation of the test cohort. Animal experimentation was approved by the institutional ethical committee; training cohort and ASO administration approved by the Com'Eth IGBMC-ICS (APAFIS#5453-2016052510176016 v5) and test cohort approved by the CREMEAS Chronobiotron (20183-2019040817583412 v5 and v6). Test cohort mice were analyzed from 3 weeks of age, n=20 *Mtm1*$^{-/y}$ mice. For both the training and test cohorts, daily observation was performed when necessary. In the case of severe phenotype, a scoring was performed to determine if action was needed to reduce pain, or if humane endpoints were reached, the mice were sacrificed. Mice were humanely sacrificed when required according to national and European legislations on animal experimentation. Male mice were analyzed in this study. Animals were housed in a temperature-controlled room (19–22°C) with a 12:12h light/dark cycle, with free access to food. See supplementary table 2 for additional information.

Antisense oligonucleotides (ASO). ASO were chemically modified with phosphorothioate in the backbone and cEt modifications on the wings with a deoxy gap (3-10-3 design). ASO were synthesized by IONIS Pharmaceuticals as previously described (Tasfaout et al. 2017). Both the 16 nucleotide ASO candidate targeting murine *Dnm2* (DYN101-m, GGCATAAGGTCACGGA) and the control sequence with no homology to the mouse genome (ASO-Ctrl; GGCCAATACGCCGTCA) were previously validated (Tasfaout et al. 2017; Buono et al. 2018). ASOs were dissolved in filtered and autoclaved sterile D-PBS (Life Technologies, #14190-144). Intraperitoneal injections of 6.25, 12.5 or 25mg/kg of ASO were performed in *Mtm1*$^{-/y}$ or wild type male mice weekly, from 5-12 weeks of age, n=7 mice/group. Mice were sacrificed 2 days after the final injection (Koch et al. 2020).

Generation of mouse cohorts. Training cohort data was generated from historical data of *Mtm1*$^{-/y}$ mice located at the IGBMC animal facility, Illkirch, France (Koch et al. 2020). The test cohort was derived as follows: in vitro fertilization (IVF) was performed (Janvier Laboratories, Rennes, France) with samples taken from *Mtm1*$^{-/y}$ mice from the colony used to generate the training cohort. IVF and colony generation was performed here, and then transferred to Chronobiotron animal facility (Strasbourg, France), for colony amplification and phenotyping (test cohort).

Disease Severity Score (DSS) analysis. DSS was performed to monitor the clinical appearance of *Mtm1*$^{-/y}$ mice. The DSS was designed to evaluate the clinical evolution of six indicators of myopathy in mice; body weight difference, hanging test ability, kyphosis, hindlimb position whilst walking, breathing ability, and ptosis, as described previously (Tasfaout et al. 2017). Details of DSS analysis, both previous and updated method based on analysis performed in this study, are represented in table 1.

Hanging test. Mice were placed on a grid (cage lid, dimensions 410 x 270 mm) which was then inverted and held 40 cm above the cage litter; the latency to fall was measured three times for each mouse, with a minimum of 5 minutes interval between trials to allow a recovery period. The latency time measurements began from the point when the mouse was hanging free on the grid and ended with the animal falling to the cage underneath the grid. The maximum time measured was 60 seconds. Results are expressed as an average of three trials.

Statistics and modelling. For the 'training cohort', historical data was accessed, where the sample size (n) was established for each individual study (Koch et al. 2020). For the 'test cohort', we calculated the statistical power using R software function "pwr2::ss.1way" (k: Number of groups; alpha; beta; f: effect size; delta: smallest difference among k group; sigma: Standard deviation, i.e. square root of variance and B: iteration times). The statistical power was calculated as n=15 for the 'test cohort' to see a difference between groups, however n=20 was used to optimally model the progression of the disease in *Mtm1*$^{-/y}$ mice. For the 'dose-response' antisense oligonucleotide study, the pre-specified effect size was established to be n=7 (Tasfaout et al. 2017).

To model body weight progression, a joint model considering survival and body weight progression was used. The evolution was not linear with time but rather changed as the square-root of weeks and the log-weight is modeled in order to account for the natural lower bound at 0. Random slopes and intercept for each mouse are included. See supplementary information for a more detailed description of the Joint Models, including for DSS Scores. Correlation analyses were performed with a Spearman or Pearson correlation test, as noted in the figure legends. Additional statistical analyses were performed as stated in the figure legend where appropriate, with p values of <0.05 considered significant. The normality of the residuals and the variance homogeneity was assessed to apply the appropriate statistical test with GraphPad Prism 9.

Exclusion criteria. All exclusion/inclusion criteria were pre-established. All male mice from 3 weeks old were included. For the dose-response study, mice entered the study at 3 weeks of age, however mice that died or were sacrificed for humane endpoints before starting the injection protocol at 5 weeks old were excluded and replaced. For sample analysis, the exclusion criteria were (1) technical issues not allowing the data to be measured; or (2) sample(s) detected as an outlier with GraphPad Prism 9 (parameters: ROUT, Q=5%).

Randomization and blinding. For the dose-response experiment, *Mtm1*$^{-/y}$ or WT mice were randomly assigned to groups at 3 weeks of age, n=7 mice per group. *Mtm1*$^{-/y}$ or WT mice from the same litter were kept in the same cage. Where possible mice from the same litter were allocated to different dosing groups. For the histological analyses in the dose-response study, the ASO dose administered was blinded to avoid any bias.

Quantitative RT-PCR. RNA was isolated from organs using NucleoSpin RNA kit (Macherey Nagel). For muscle tissue, the supplementary protocol available from the manufacturer entitled “isolation of RNA from fibrous tissue” was used. Reverse transcription was carried out on 250 ng aliquot using SuperScript™ IV Reverse Transcriptase (Thermofisher Scientific). qPCR was done with PowerUp™ SYBR™ Green Master Mix (ThermoFisher Scientific) in a Quant Studio 3 Real-Time PCR System (ThermoFisher Scientiifc). The relative expression of *Dnm2* mRNA was normalized to *Rpl27*. Primers used: *Rpl27* Forward 5’-AAGCCGTCATCGTGAAGAACA-3’, *Rpl27* Reverse 5’ CTTGATCTTGGATCGCTTGGC-3’, *Dnm2* Forward 5’ACCCCACACTTGCAGAAAAC-3’, *Dnm2* Reverse 5’CGCTTCTCAAAGTCCACTCC-3’. mRNA analysis followed most MIQE standards.

Histological analysis of skeletal muscle. Air dried transverse cryosections (8 µm) were fixed and stained with hematoxylin and eosin (HE) or succinate dehydrogenase (SDH), and image acquisition performed with a slide scanner NanoZoomer 2 HT equipped with the brightfield and the fluorescence module L11600-21 (Hamamatsu Photonics, Japan). Minimum feret’s diameter was analyzed in wheat germ agglutinin (WGA) sections from TA mouse skeletal muscle, using a plugin developed in ImageJ – ‘MyoMage’. Minimum feret’s diameter was calculated in >500 fibers per mouse. The percentage of TA muscle fibers with centralized or internalized nuclei was counted in >500 fibers using the cell counter plugin in ImageJ (Rasband, W.S., ImageJ, U. S. National Institutes of Health, Bethesda, Maryland, USA, http://rsb.info.nih.gov/ij/, 1997-2009) or FIJI analysis software. Qualitative SDH staining analysis was

performed. Fiber to fiber variation in intensity in SDH staining is normal and is indicative of the oxidative state of the fiber. SDH staining is normally relatively homogenous within each individual fiber. Accumulation within the center or the periphery of a fiber of SDH staining indicates an abnormal distribution.

Acknowledgements: We thank the animal house of the IGBMC and Chronobiotron (part of the CELPHEDIA group (http://www.celphedia.eu), for support. Thank you to Shuling Guo and Brett Monia for providing reagents and advice. Thank you to Pascal Kessler for providing the ImageJ plugin MyoMage.

Competing interests: B.S.C and J.L. are coinventors of a patent on targeting DNM2 for the treatment of centronuclear myopathies, and cofounders of Dynacure. B.S.C, C.K., S.B., A.M., A.R., M.D. and L.T. are currently employed by Dynacure.

Funding: This study was funded by Dynacure, and supported by a Be Est Projets d'Avenir' du programme d'Investissement Avenir 3 awarded grant (coDyn101) to BSC.

Data availability: No high throughput experiments, novel sequences, or publicly referenced databases were used in this manuscript. Model formulas can be found in the supplementary data of this paper. Wild type and *Mtm1*$^{-/y}$ datasets will be made available upon request.

Author contributions statement: BSC designed the study. SB, AM, and AR performed experiments, AR performed statistical analysis, CK provided technical support, MD, LT, JL, provided scientific advice, BSC directed the research and wrote the manuscript with input from all coauthors.

References

Buj-Bello, A., F. Fougerousse, Y. Schwab, N. Messaddeq, D. Spehner, C. R. Pierson, M. Durand, C. Kretz, O. Danos, A. M. Douar, A. H. Beggs, P. Schultz, M. Montus, P. Denefle, and J. L. Mandel. 2008. 'AAV-mediated intramuscular delivery of myotubularin corrects the myotubular myopathy phenotype in targeted murine muscle and suggests a function in plasma membrane homeostasis', *Hum Mol Genet*, 17: 2132-43.

Buj-Bello, A., V. Laugel, N. Messaddeq, H. Zahreddine, J. Laporte, J. F. Pellissier, and J. L. Mandel. 2002. 'The lipid phosphatase myotubularin is essential for skeletal muscle maintenance but not for myogenesis in mice', *Proc Natl Acad Sci U S A*, 99: 15060-5.

Buono, S., J. A. Ross, H. Tasfaout, Y. Levy, C. Kretz, L. Tayefeh, J. Matson, S. Guo, P. Kessler, B. P. Monia, M. Bitoun, J. Ochala, J. Laporte, and B. S. Cowling. 2018. 'Reducing dynamin 2 (DNM2) rescues DNM2-related dominant centronuclear myopathy', *Proc Natl Acad Sci U S A*, 115: 11066-71.

Cowling, B. S., T. Chevremont, I. Prokic, C. Kretz, A. Ferry, C. Coirault, O. Koutsopoulos, V. Laugel, N. B. Romero, and J. Laporte. 2014. 'Reducing dynamin 2 expression rescues X-linked centronuclear myopathy', *J Clin Invest*, 124: 1350-63.

Cowling, B. S., and L. Thielemans. 2019. 'Translational medicine in neuromuscular disorders: from academia to industry', *Dis Model Mech*, 13.

Cowling, B. S., A. Toussaint, L. Amoasii, P. Koebel, A. Ferry, L. Davignon, I. Nishino, J. L. Mandel, and J. Laporte. 2011. 'Increased expression of wild-type or a centronuclear myopathy mutant of dynamin 2 in skeletal muscle of adult mice leads to structural defects and muscle weakness', *Am J Pathol*, 178: 2224-35.

Daniele, N., C. Moal, L. Julien, M. Marinello, T. Jamet, S. Martin, A. Vignaud, M. W. Lawlor, and A. Buj-Bello. 2018. 'Intravenous Administration of a MTMR2-Encoding AAV Vector Ameliorates the Phenotype of Myotubular Myopathy in Mice', *J Neuropathol Exp Neurol*, 77: 282-95.

Gayi, E., L. A. Neff, X. Massana Munoz, H. M. Ismail, M. Sierra, T. Mercier, L. A. Decosterd, J. Laporte, B. S. Cowling, O. M. Dorchies, and L. Scapozza. 2018. 'Tamoxifen prolongs survival and alleviates symptoms in mice with fatal X-linked myotubular myopathy', *Nat Commun*, 9: 4848.

Gordish-Dressman, H., R. Willmann, L. Dalle Pazze, A. Kreibich, M. van Putten, A. Heydemann, L. Bogdanik, C. Lutz, K. Davies, A. R. Demonbreun, D. Duan, D. Elsey, S. I. Fukada, M. Girgenrath, J. Patrick Gonzalez, M. D. Grounds, A. Nichols, T. Partridge, M. Passini, F. Sanarica, F. J. Schnell, D. J. Wells, T. Yokota, C. S. Young, Z. Zhong, C. Spurney, M. Spencer, A. De Luca, K. Nagaraju, and A. Aartsma-Rus. 2018. '"Of Mice and Measures": A Project to Improve How We Advance Duchenne Muscular Dystrophy Therapies to the Clinic', *J Neuromuscul Dis*, 5: 407-17.

Koch, C., S. Buono, A. Menuet, A. Robe, S. Djeddi, C. Kretz, R. Gomez-Oca, M. Depla, A. Monseur, L. Thielemans, L. Servais, C. N. M. Study Group NatHis, J. Laporte, and B. S. Cowling. 2020. 'Myostatin: a Circulating Biomarker Correlating with Disease in Myotubular Myopathy Mice and Patients', *Mol Ther Methods Clin Dev*, 17: 1178-89.

Laporte, J., L. J. Hu, C. Kretz, J. L. Mandel, P. Kioschis, J. F. Coy, S. M. Klauck, A. Poustka, and N. Dahl. 1996. 'A gene mutated in X-linked myotubular myopathy defines a new putative tyrosine phosphatase family conserved in yeast', *Nat Genet*, 13: 175-82.

Liu, N., S. Bezprozvannaya, J. M. Shelton, M. I. Frisard, M. W. Hulver, R. P. McMillan, Y. Wu, K. A. Voelker, R. W. Grange, J. A. Richardson, R. Bassel-Duby, and E. N. Olson. 2011. 'Mice lacking microRNA 133a develop dynamin 2-dependent centronuclear myopathy', *J Clin Invest*, 121: 3258-68.

Maani, N., N. Sabha, K. Rezai, A. Ramani, L. Groom, N. Eltayeb, F. Mavandadnejad, A. Pang, G. Russo, M. Brudno, V. Haucke, R. T. Dirksen, and J. J. Dowling. 2018. 'Tamoxifen therapy in a murine model of myotubular myopathy', *Nat Commun*, 9: 4849.

Massana Munoz, X., S. Buono, P. Koebel, J. Laporte, and B. S. Cowling. 2019. 'Different in vivo impacts of dynamin 2 mutations implicated in Charcot-Marie-Tooth neuropathy or centronuclear myopathy', *Hum Mol Genet*, 28: 4067-77.

Ravenscroft, G., N. G. Laing, and C. G. Bonnemann. 2015. 'Pathophysiological concepts in the congenital myopathies: blurring the boundaries, sharpening the focus', *Brain*, 138: 246-68.

Shieh, P. B., C. G. Bonnemann, W. Muller-Felber, A. Blaschek, J. J. Dowling, N. L. Kuntz, and A. M. Seferian. 2020. 'Re: "Moving Forward After Two Deaths in a Gene Therapy Trial of Myotubular Myopathy" by Wilson and Flotte', *Hum Gene Ther*, 31: 787.

Tasfaout, H., S. Buono, S. Guo, C. Kretz, N. Messaddeq, S. Booten, S. Greenlee, B. P. Monia, B. S. Cowling, and J. Laporte. 2017. 'Antisense oligonucleotide-mediated Dnm2 knockdown prevents and reverts myotubular myopathy in mice', *Nat Commun*, 8: 15661.

Tasfaout, H., V. M. Lionello, C. Kretz, P. Koebel, N. Messaddeq, D. Bitz, J. Laporte, and B. S. Cowling. 2018. 'Single Intramuscular Injection of AAV-shRNA Reduces DNM2 and Prevents Myotubular Myopathy in Mice', *Mol Ther*, 26: 1082-92.

van Putten, M., K. Putker, M. Overzier, W. A. Adamzek, S. Pasteuning-Vuhman, J. J. Plomp, and A. Aartsma-Rus. 2019. 'Natural disease history of the D2-mdx mouse model for Duchenne muscular dystrophy', *FASEB J*, 33: 8110-24.

Vandersmissen, I., V. Biancalana, L. Servais, J. J. Dowling, G. Vander Stichele, S. Van Rooijen, and L. Thielemans. 2018. 'An integrated modelling methodology for estimating the prevalence of centronuclear myopathy', *Neuromuscul Disord*, 28: 766-77.

Willmann, R., J. Lee, C. Turner, K. Nagaraju, A. Aartsma-Rus, D. J. Wells, K. R. Wagner, C. Csimma, V. Straub, M. D. Grounds, and A. De Luca. 2020. 'Improving translatability of preclinical studies for neuromuscular disorders: lessons from the TREAT-NMD Advisory Committee for Therapeutics (TACT)', *Dis Model Mech*, 13.

Fgures and Table

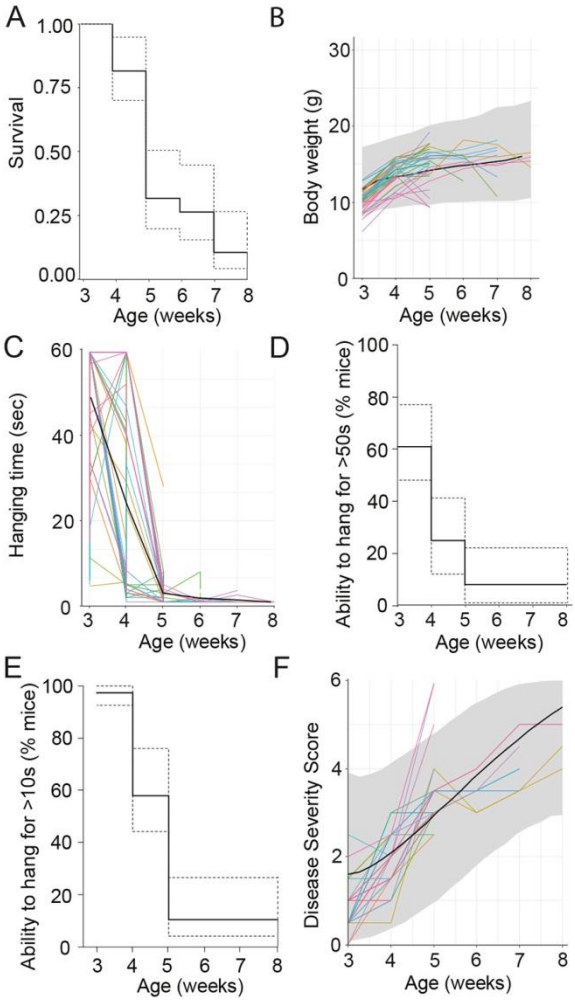

Figure 1. Natural history study analysis and model generation from training cohort. (A) Survival of mice, line of best fit (solid line) and 95% confidence interval (dotted line) shown. (B) Body weight (grams) progression weekly in *Mtm1*$^{-/y}$ mice. Individual mice shown (colored lines), line of best fit (black) and prediction interval (shaded grey zone), are highlighted on the graph. (C) Hanging time (60 seconds maximum), with individual mice progression (colored lines) and average (black line) shown. Time to event analysis of hanging test shown, with cutoff times of 50 seconds (D) and 10 seconds (E) displayed. Graphs represent line of best fit (solid line) ±95%CI (dotted line). (F) Disease severity score, with a score between 0 (unaffected) and 6 (most severely affected) awarded per mouse per week, based on 6 different phenotypes (see table 1 for details). Modelling was performed to identify the line of best fit (black), and prediction intervals (grey shaded area) for expected disease progression in *Mtm1*$^{-/y}$ mice. All mice data in this figure represent analysis of *Mtm1*$^{-/y}$ mice phenotypes from the training cohort, from 3 weeks of age, individual mice represented as colored lines. N=38 male mice.

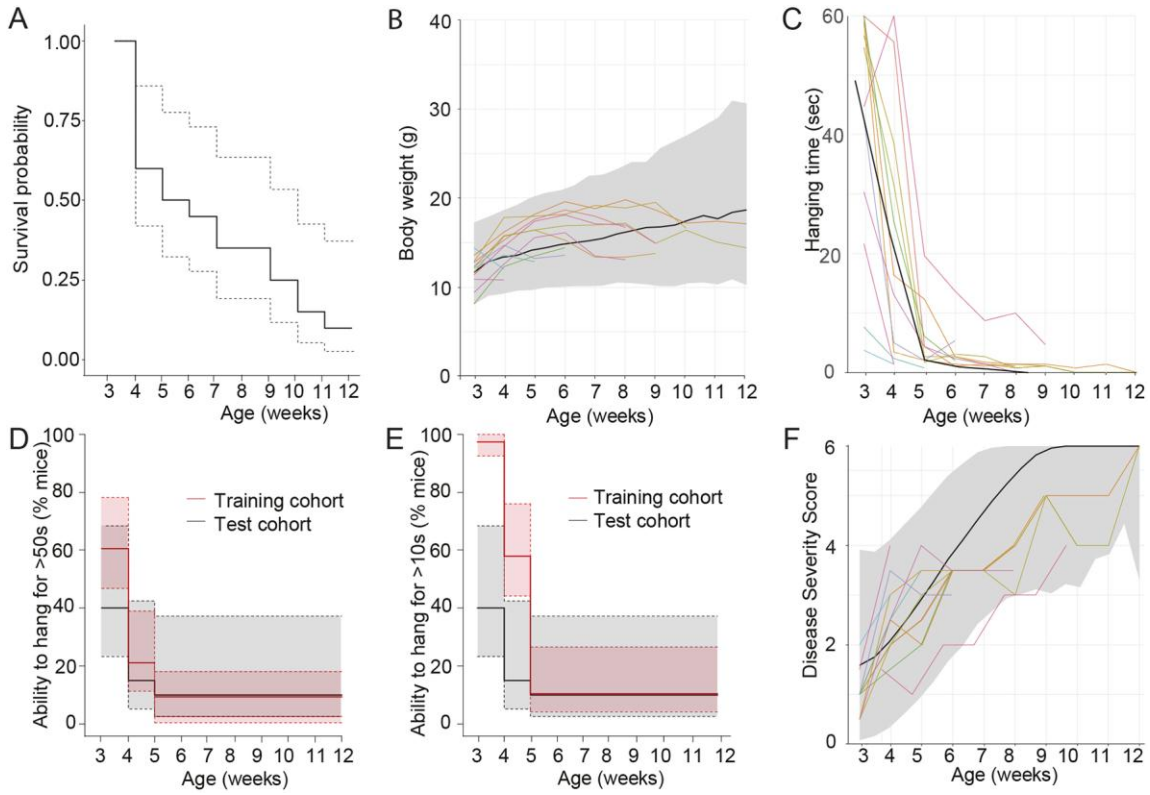

Figure 2: Natural history study in test cohort of *Mtm1*$^{-/y}$ mice. (A) Survival of mice, line of best fit (solid line) and 95% confidence interval (dotted line) shown. (B) Body weight (grams) progression weekly in *Mtm1*$^{-/y}$ mice. Individual mice shown (colored lines), and line of best fit (black) and prediction interval (shaded grey zone), from training cohort (Figure 1B) are highlighted on the graph. (C) Hanging time (60 seconds maximum), with individual mice progression shown (colored lines). The line of best fit from the training cohort (Figure 1C) highlighted in black. Time to event analysis of hanging test shown, with cutoff times of 50 seconds (D) and 10 seconds (E) displayed. Graphs represent line of best fit (solid line) ±95%CI (dotted line) of training (red, from Figure 1D,E) and test (black) cohorts for comparison. (F) Disease severity score, with a score between 0 (unaffected) and 6 (most severely affected) awarded per mouse per week, based on 6 different phenotypes (see table 1 for details). Line of best fit (black), and prediction intervals (grey shaded area) are shown from training cohort for reference (Figure 1F). All mice data in this figure represent analysis of *Mtm1*$^{-/y}$ mice phenotypes from the test cohort, from 3 weeks of age, individual mice represented as colored lines. N=20 male mice.

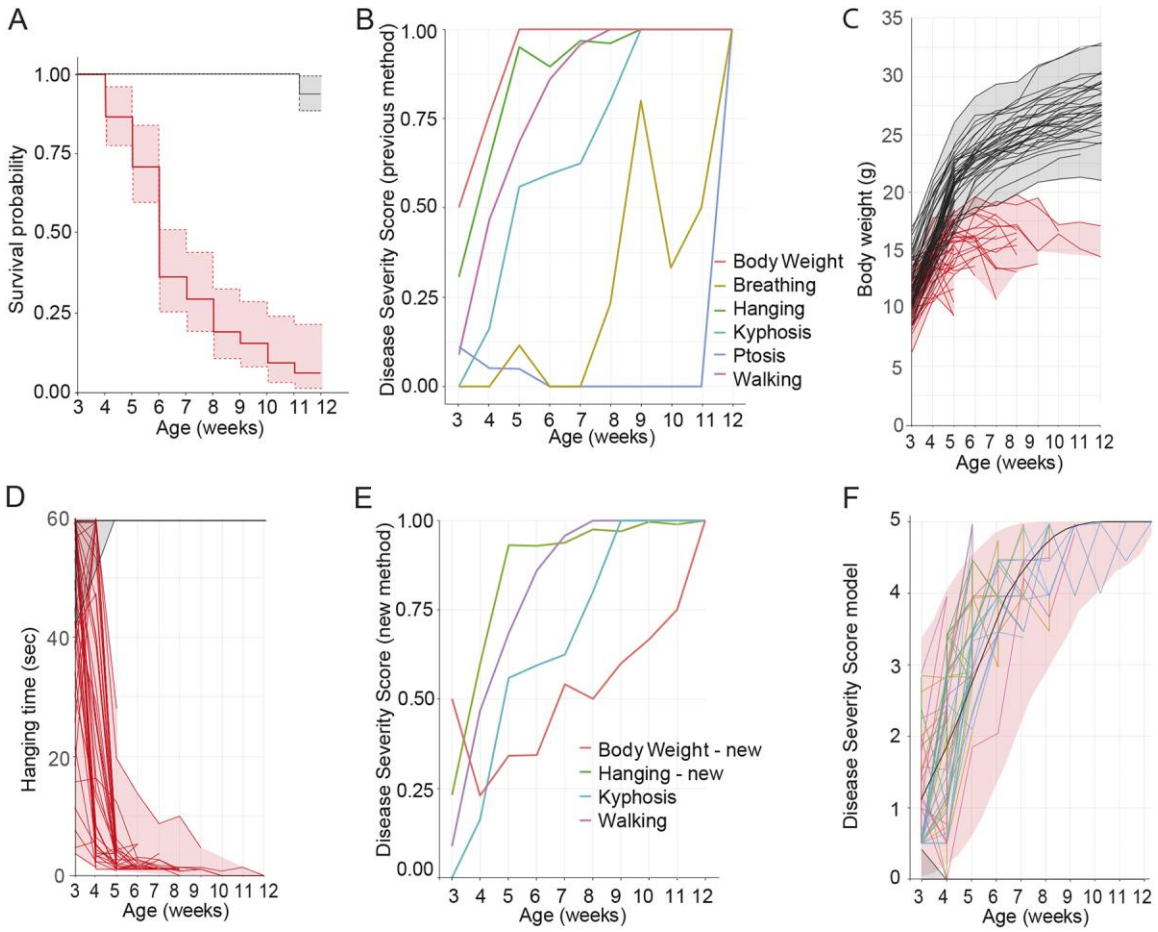

Figure 3: Optimized Disease Severity Analysis based on combined natural history study data from training and test cohorts. (A) Survival of mice, line of best fit (solid line) and 95% confidence interval (dotted line) shown for wildtype (black) and *Mtm1*$^{-/y}$ mice (red). (B) Line of best fit shown for progression of each of the 6 individual factors comprising the disease severity score for *Mtm1*$^{-/y}$ mice (see table 1 for details). Individual body weight (C) and hanging time (D) from combined natural history study data from training and test cohorts for wildtype (black) and *Mtm1*$^{-/y}$ mice (red). (E) Line of best fit shown for progression of each of the selected 4 individual factors comprising the optimized disease severity score in *Mtm1*$^{-/y}$ mice (see table 1 for details). (F) Disease severity score progression of individual *Mtm1*$^{-/y}$ mice, with a score between 0 (unaffected) and 5 (most severely affected) awarded per mouse per week, based on 4 different phenotypes (see table 1 for details, hanging test maximal value of 2 possible). Line of best fit (black), and prediction intervals (shaded area) modelling is shown. All wildtype mice had a score of 0 from week 4 onwards (black line, shading). All mice data in this figure represent analysis of wild type (n=64) and *Mtm1*$^{-/y}$ (n=58) mice phenotypes from the training and test cohorts, from 3 weeks of age, individual mice represented as colored lines.

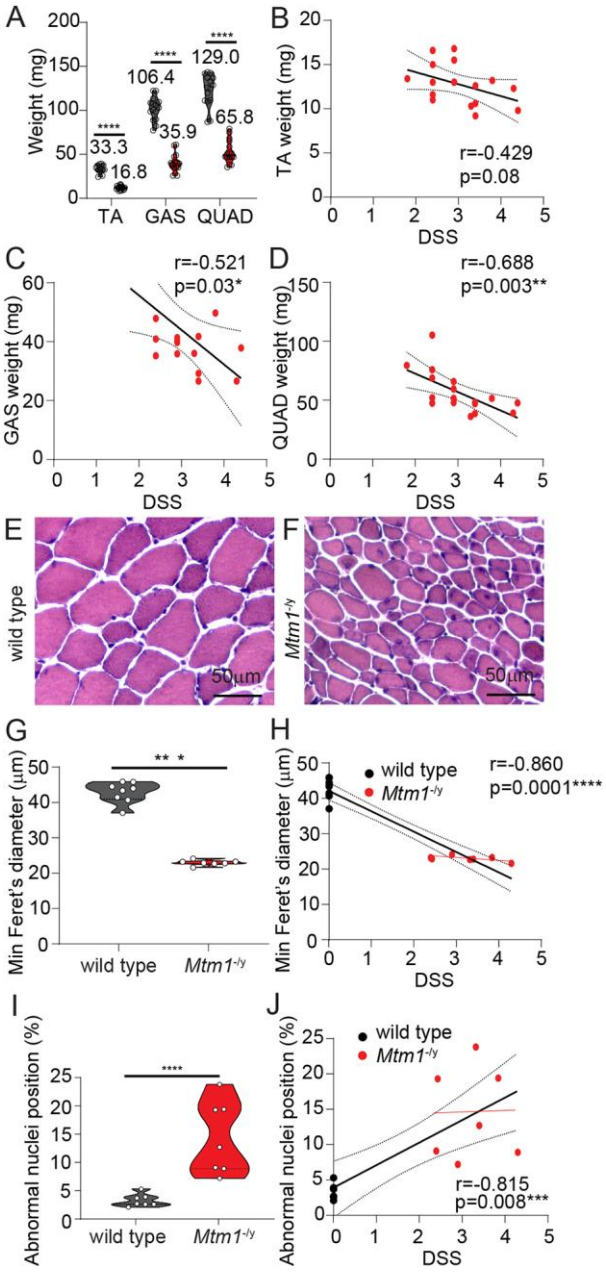

Figure 4. Skeletal muscle analysis relative to disease severity in *Mtm1*$^{-/y}$ mice. (A) Muscle mass of tibialis anterior (TA), gastrocnemius (GAS) and quadriceps (QUAD) muscles from wildtype and *Mtm1*$^{-/y}$ mice. Correlation analysis of TA (B), GAS (C) and QUAD (D) muscle mass relative to disease severity score (DSS) for *Mtm1*$^{-/y}$ mice. Line of best fit and 95%CI highlighted. Representative hematoxylin and eosin (HE) staining of TA muscles from wild type (E) and *Mtm1*$^{-/y}$ mice (F). Analysis of fiber size, represented as minimum feret's diameter presented alone (G), or relative to DSS (H). Analysis of fibers with altered nuclei positioning presented alone (I) or relative to DSS (J). (H,J) Line of best fit and 95%CI highlighted for all mice (black), and line of best for *Mtm1*$^{-/y}$ mice alone (red). (A,F,H) Represented as a violin plots, individual mouse data shown. Spearman correlation analysis performed for (C), (D), (H), (J); Pearson correlation analysis for (B); unpaired t-test for (A,TA and A,QUAD)(I); unpaired t-test with Welsh's correction for (A,GAS)(G). *p<0.05, **p<0.01, ***p<0.001, ****p<0.0001.

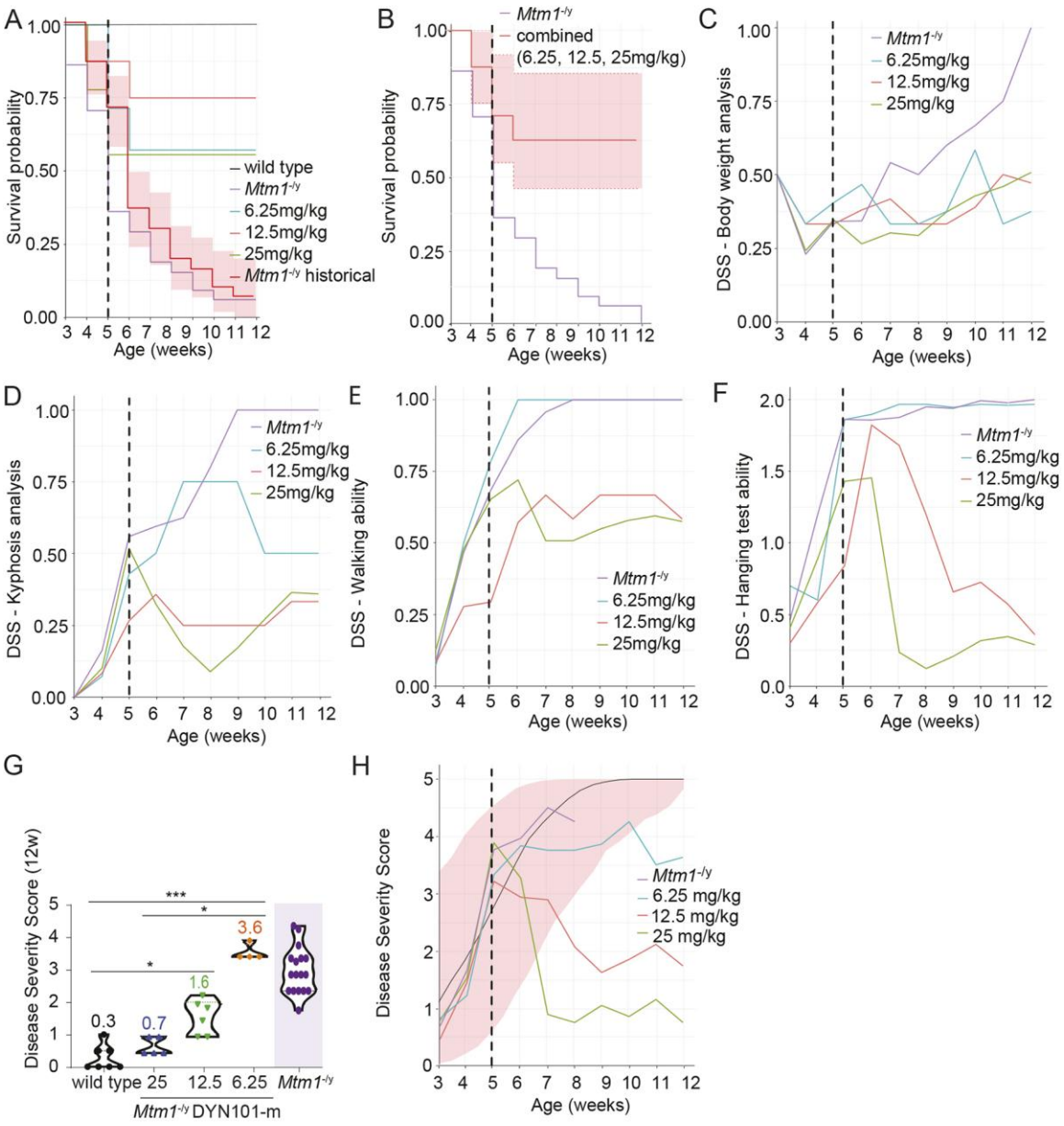

Figure 5. Validation of the model in a dose response study with DNM2 therapy. Three doses were selected; low, mid, and high (6.25, 12.5, 25mg/kg; blue, red, green lines respectively) doses of DYN101-m targeting murine *Dnm2*, were delivered weekly by intraperitoneal injection from 5-12 weeks of age to *Mtm1*$^{-/y}$ mice, and compared to wild type (black), and *Mtm1*$^{-/y}$ control mice injected with ASO control (purple), n=7 mice/group. Survival of mice shown for all groups separately (A), or with DYN101-m treated groups combined (B). Average (solid line) and 95% confidence interval (dotted line) shown for grouped data (B). Individual progression (average) of individual disease severity score factors; body weight analysis (C), kyphosis (D), walking ability (E), and hanging test performance (F). (G) Disease severity score of wild type and *Mtm1*$^{-/y}$ mice at 12 weeks of age, with a score between 0 (unaffected) and 5 (most severely affected) awarded per mouse, based on 4 different phenotypes (C-F). DYN101-m dosing indicated where relevant (mg/kg). DSS from *Mtm1*$^{-/y}$ mice at 7 weeks of age from figure 4 shown for reference only (purple). (H) Disease severity score model (Figure 3D) represented by line of best fit

(black), and prediction intervals (shaded area) modelling is displayed; line of best fit for joint-longitudinal survival and phenotyping of *Mtm1*$^{-/y}$ mice (control, low, mid, high dose) in the dose-response study indicated. Dashed black line indicates time of first injection. Kruskal-Wallis test performed for (G). **p*<0.05, ***p*<0.01, ****p*<0.001, *****p*<0.0001.

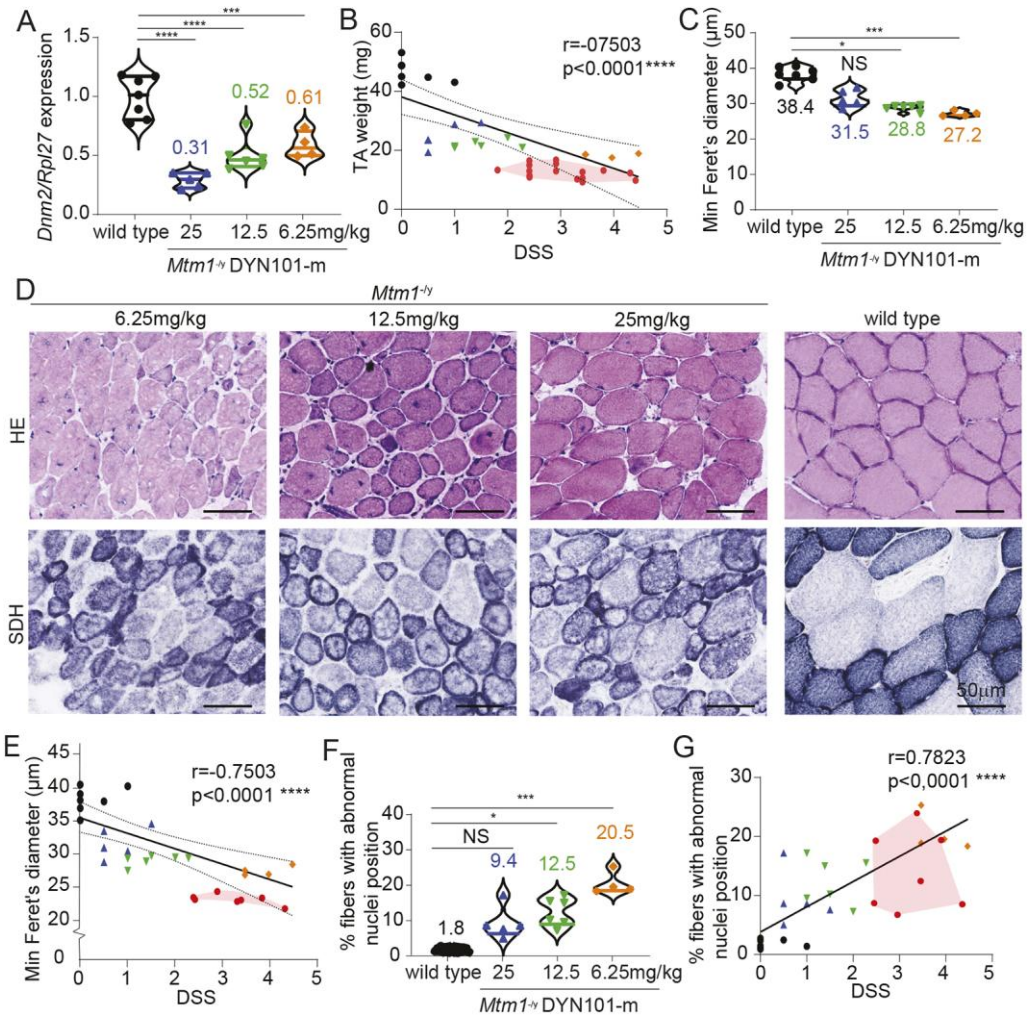

Figure 6. Correlation analysis of post mortem skeletal muscle specimens with disease severity following DNM2 therapy. (A) *Dnm2* mRNA expression quantified by qRT-PCR analysis, relative to *Rpl27* expression, from tibialis anterior muscles, represented as mean±SD. Ordinary 1-way ANOVA followed by Dunnett's multiple comparisons test performed. (B) Tibialis anterior muscle mass relative to disease severity score (DSS). Analysis of fiber size, represented as minimum feret's diameter alone (C), or relative to DSS (E). (D) Hematoxylin and eosin (HE, upper panel) and succinate dehydrogenase (SDH, lower panel) staining of tibialis anterior muscles (scale bar = 50µm). Analysis of fibers with altered nuclei positioning displayed alone (F) or relative to DSS (G). (A, C, F) Represented as a violin plots, individual mouse data shown, n=4-7 mice per group. (C,F) Kruskal-Wallis (non-parametric) followed by Dunn's multiple comparisons test performed. Spearman correlation tests performed for (B), (E), (G). 12 week old *Mtm1*$^{-/y}$ mice injected with 6.25, 12.5, or 25mg/kg are represented by orange, green, and blue points respectively, wild type mice by black dots. Figure (B), (E) and (G) contain as an overlay *Mtm1*$^{-/y}$ mice at 5 weeks of age, reproduced from figure 4, purely for comparative purposes, and are not included in statistical analyses here. **p*<0.05, ***p*<0.01, ****p*<0.001,, *****p*<0.0001.

Table 1: Disease severity scoring system factors. Previous disease severity scoring system (Tasfaout et al. 2017), and optimized disease severity scoring system based on NHS data analysis and modeling from training and test cohorts of *Mtm1*$^{-/y}$ mice. The full Standard Operating Procedure can be found in supplementary information of this manuscript.

Disease scoring factor	Previous DSS - Description (from Tasfaout et al 2017)	Score	Optimized DSS - Description	Score
Body weight	Difference in body weight between *Mtm1*$^{-/y}$ mouse and wildtype littermate	0: 0-1g 0.5: >1-2g 1: >2g	Difference in body weight between *Mtm1*$^{-/y}$ mouse from week n to n+1 is:	0: >0.25g gain 0.5: ±0-0.25g* 1: >0.25g loss
Breathing difficulties			Not included	
Hanging test ability	Ability to hang from the lid of a cage for 60 seconds	0: 60s 0.5: 5-60s 1: <5	As before, with score of 0-2, representing 0-60 seconds hanging time.	(60-Time (s))/60s*2 = value (0-2) Examples: 1s -> (60-1)/60*2=1.97 15s -> (60-15)/60*2=1.5 30s -> (60-30)/60*2=1 60s -> (60-60)/60*2=0
Kyphosis	Curvature of the spine	0: No 0.5: Mild 1: Severe	Unchanged	
Ptosis	Drooping of the eyelid	0: No 0.5: X 1: Yes	Not included	
Walking difficulties	Ability to use hindlimbs	0: Normal 0.5: Splayed 1: Loss of use	Unchanged	
Maximum score		6		5

*relevant during growth phase of a mouse, from 0-12 weeks.

Supplementary materials and Methods

Joint Models for Disease Severity Scores. Joint models for disease severity scores are presented in the associated manuscript. The mice where followed over a period $[0; \tau\ [$. For each subject i, we observe the following:

- Longitudinal measures: $\{Y_{ij}; j = 1, \dots, n_i\}$ at times $\{t_{ij}\,; j = 1, \dots, n_i\}$
- Survival time and indicator:

$$T = \min(ST, C) \text{ and } \delta = I(ST \leq C) = \begin{cases} 1\ if\ uncensored\ observation \\ 0\ if\ censored\ observation \end{cases}$$

The longitudinal measurements and time to event were jointly measured via a latent bivariate process, which was realized independently in each subject $W_i = \{W_{1i_i}, W_{2i}\}$

The longitudinal sub-model is defined as: The observed response y_{ij} scaled between 0 and 1 ($i = 1, \dots, M\ and\ j = 1, \dots, n_i$), is defined as :$y_{ij} \sim Beta(a_{ij}, b_{ij})$; where the beta distribution is defined by the parameters a_{ij} and b_{ij} , which are defined, respectively, by the mean μ_{ij} and "the sample size" ν of the distribution as follows:

$$a_{ij} = \mu_{ij} * \nu$$
$$b_{ij} = (1 - \mu_{ij}) * \nu$$

The parameter ν is estimated from the data, and the mean μ_{ij} is defined as a mixed model with logit-link function, where *T* is a constant to center time:

$$\chi_{ij} = \alpha_i + \beta * (T + t_{ij})$$
$$\mu_{ij} = \frac{1}{1 + exp\,(-\chi_{ij})}$$

The equation of the mean contains a random effect on the intercept $W_{1i} = \alpha_i \sim N(0, \sigma_\alpha^2)$. In turn, the survival sub-model is then defined via a Weibull survival model:

$$S(t_{ij}) = \exp\,(-(\zeta_i * t_{ij})^k)$$

Where:

$$\zeta_i = \exp(-W_{2i})$$
$$W_{2i} = \gamma * \alpha_i$$

Where γ expresses the induced association. A negative value of gamma implies that the larger value of the DSS Score the smaller the probability to stay in the study. A positive value would however imply the opposite. For simplicity in estimation, k = 1 in all estimations of the model indicating a constant failure rate. The model for the evolution of weight over time is similar to the one proposed here over.

The main difference lies in the equation for the mean. Indeed, the equation is assumed to be a linear gaussian model that evolves a the square root of time rather than a beta model.

The disease severity data from individual mice are included only until the point of death. The death of the mouse is then factored into the joint longitudinal survival model for disease severity scores. The above model used here allows the expected range to be presented following the correction for limited sample size, variability, and survival differences. The output is presented as the line of best fit (black line) and prediction intervals (shaded zone). A correct model fit occurs when 95% of the observed individual data is contained, for each time point, in the intervals depicted. Individual data from all living mice is shown as an overlay of the model to confirm this point on each graph, and thus the validity of the model.

Table S1. Previous Disease severity scoring system (Tasfaout, Buono et al. 2017). A scoring system was set up to evaluate the clinical evolution of six centronuclear myopathy features. Difference of body weight between *Mtm1*$^{-/y}$ versus WT littermate, ability to perform the hanging test, walking manner, presence or absence of ptosis and kyphosis and breathing difficulties (frequency and amplitude evaluation based on clinical observations) are recorded and a score of 0, 0.5 or 1 is given to each clinical readout. The sum represents the DSS. The higher the DSS, the more severe the phenotype, minimum 0 (healthy mouse), maximum 6 (severely affected mouse) (Tasfaout, Buono et al., 2017).

Disease scoring category	DSS Description	Score
Body weight	Score 0-1 Difference in body weight between *Mtm1*$^{-/y}$ mouse and wildtype littermate	0: 0-1g 0.5: >1-2g 1: >2g
Ptosis	Score 0 or 1 Drooping of the eyelid	0 : No 1 : Yes 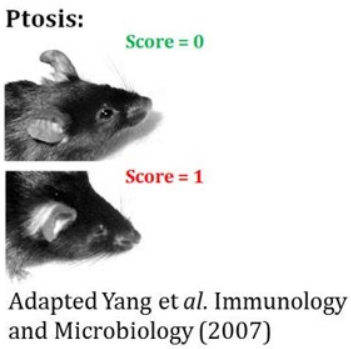 Adapted Yang et *al.* Immunology and Microbiology (2007)
Hanging test ability	Score of 0-1, representing 0-60 seconds hanging time.	0: 60s 0.5: 5-60s 1: <5

Kyphosis	Score 0-1 Curvature of the spine	Score 0: no curvature of the spine Score 0.5: mild curvature of the spine 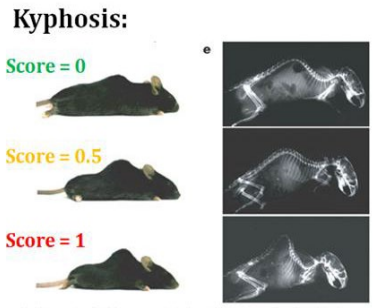 Adapted from Gabellini et *al.* Nature (2006) Score 1: severe curvature of the spine
Breathing difficulties	Score 0 or 1 Frequency and amplitude evaluation based on clinical observations	0: no breathing alternation 1: breathing alternation
Walking difficulties	Score 0-1 Ability to use hindlimbs	Score 0: normal use of hindlimbs Score 0.5: splayed use of hindlimbs Score 1: loss of use of hindlimbs 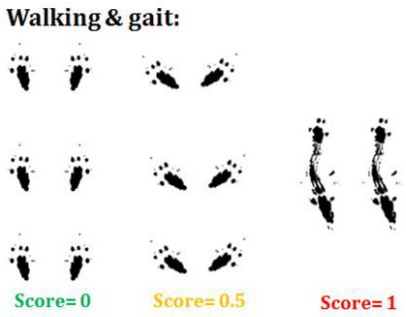
Maximum score	6	

Table S2. Husbandry and housing conditions for training and test cohorts

	TRAINING COHORT	TEST COHORT
	Training cohort data was generated from historical data of *Mtm1*$^{-/y}$ mice located at the IGBMC animal facility, Illkirch, France (Koch, Buono et al. 2020). N=38 mice	Test cohort data: In vitro fertilization (IVF) was performed (Janvier Laboratories, Rennes, France) with samples taken from *Mtm1*$^{-/y}$ mice from the colony used to generate the training cohort. Following IVF and colony generation, mice were transferred to Chronobiotron animal facility (Strasbourg, France), for colony amplification and phenotyping (test cohort). N=20 mice
Husbandry conditions	Light cycle: 12hr/12hr Temperature: 19-22°C Enrichment: nests to help nesting.	Janvier Laboratories : Light cycle: 12hr/12hr Temperature: +21°C ± 2°C Enrichment: all cages contain sticks to gnaw (Aspenbrick). Breeding cages were systematically enriched with nests.
Housing conditions	Light cycle: 12hr/12hr Temperature: 19-22°C Enrichment: nests	Chronobiotron animal facility: Light cycle: 12hr/12hr Temperature: +21°C ± 2°C Enrichment: nests and cardboard tunnel
Weaning age	3 weeks of age	3 weeks of age
Description of cage	*Cage type 2:* Individually ventilated cages: no Floor surface: 370 cm² *Cage type 3:* For housing during experimental procedure, cage type 3 was rarely used because of the larger size and increased distance to access food Access to food and water: Gel diet was added inside the cage to facilitate access. Food pellets were added at multiple places inside the cages.	Chronobiotron animal facility: *Cage type 2:* Individually ventilated cages: no Brand: Tecniplast (#1264C Eurostandard) or Erhet Floor surface: 370 cm² Dimensions: L x W x H : 268 x 215 x 141 mm *Cage type 3:* For housing during experimental procedure, cage type 3 was rarely used because of the larger size and increased distance to access to the food. Individually ventilated cages: no Brand: Zoonlab Floor surface: 830 cm² Dimensions: L x W x H : 425 x 265 x 150 mm Access to food and water: Gel diet was added inside the cage to facilitate access. Food pellets were added at multiple places inside the cages. Longer nozzles on water bottles were used to reduce the distance between floor and bottle nozzle.
Animal density	4 animals per cage: type II cage 5 animal per cages: type III cage	4 animals per cage: type II cage 5 animal per cages: type III cage
Genotype ratio	Typically 1 or 2 wildtype mice were housed in each cage with *Mtm1*$^{-/y}$ mice from the same litter, whenever feasible.	
Change frequency	Once per week	

Diet	**Food composition:**	**SAFE® gel diet breeding**	**SAFE® gel diet water**
	Cereals	17.3%	
	Proteins	6.6%	
	Vitamins, minerals	1.2%	
	Fibers	1.4%	1.8%
	Water	72.9%	98.2%

Results

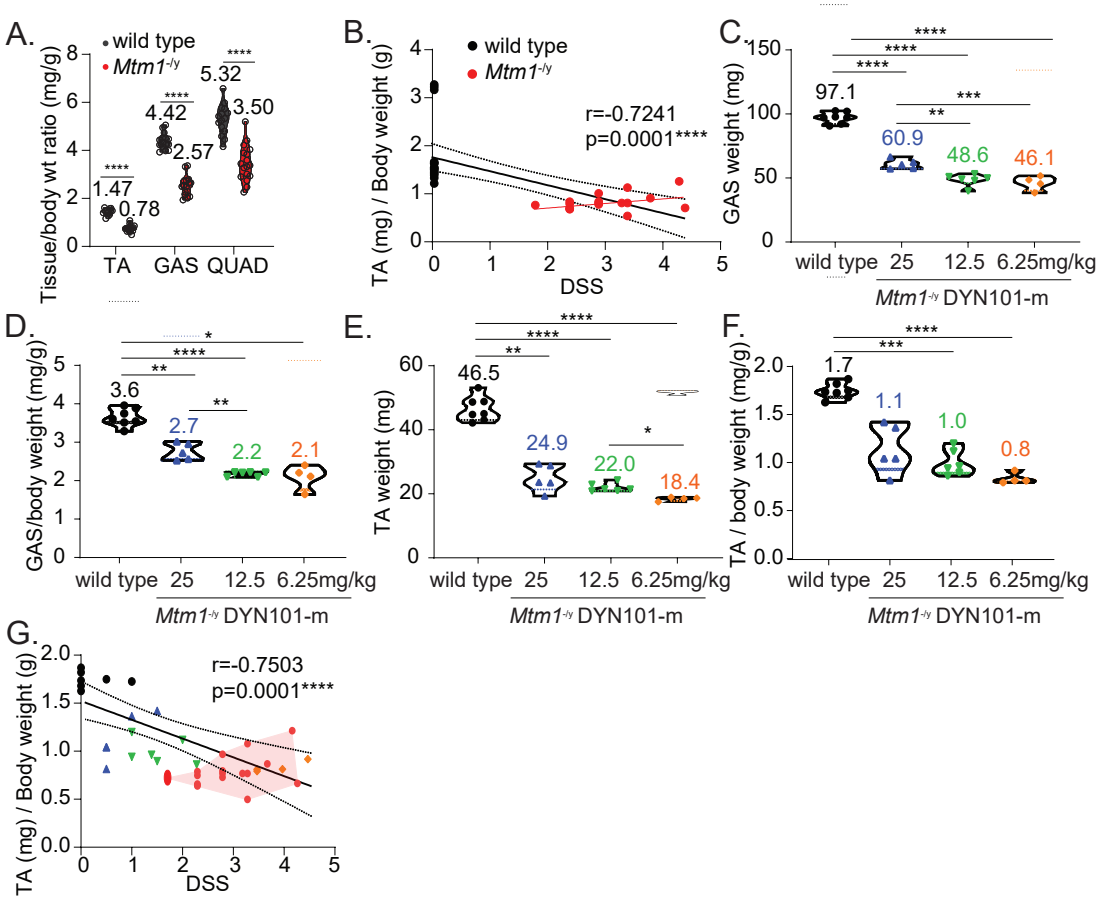

Fig. S1. Analysis of post mortem skeletal muscle speci-mens and correlation with disease severity

(A) Muscle mass of tibialis anterior (TA), gastrocnemius (GAS) and quadriceps (QUAD) muscles relative to body weight, from 5 week old wildtype and *Mtm1*$^{-/y}$ mice. Unpaired t-test with Welsh's correction performed. (B) Correlation analysis of TA muscle mass/body weight ratio, relative to disease severity score (DSS) for 5 week old *Mtm1*$^{-/y}$ (red) and wild type mice (black). Line of best fit and 95%CI highlighted in black for all mice (r= -0.7241; $p < 0.0001$), line of best fit for *Mtm1*$^{-/y}$ alone (red line). Muscle mass presented alone (GAS-C; TA-E) or relative to body weight (GAS-D; TA-F), for wildtype and *Mtm1*$^{-/y}$ mice injected with 6.25, 12.5 or 25mg/kg DYN101-m targeting murine *Dnm2* reduction. (G) TA/ body weight ratio represented relative to DSS for wild type (black), *Mtm1*$^{-/y}$ mice injected with 6.25 (orange), 12.5 (green), 25mg/kg (blue) DYN101-m. 5 week old *Mtm1*$^{-/y}$ mice from (B) reproduced here for comparison purposes only (red dots, shading), and are not included in statistical analysis. Data represented as a violin plots (A,C-F), individual mouse data shown. Statistical analysis: (A) Unpaired t-test with Welsh's correction; Spearman correlation tests performed for (B), (G) Ordinary 1-way ANOVA followed by Dunnett's multiple comparisons test performed for (C)-(F). *p<0.05, **p<0.01, ***p<0.001,, ****p<0.0001.

References

Koch, C., S. Buono, A. Menuet, A. Robe, S. Djeddi, C. Kretz, R. Gomez-Oca, M. Depla, A. Monseur, L. Thielemans, L. Servais, C. N. M. S. G. NatHis, J. Laporte and B. S. Cowling (2020). "Myostatin: a Circulating Biomarker Correlating with Disease in Myotubular Myopathy Mice and Patients." Mol Ther Methods Clin Dev **17**: 1178-1189.

Tasfaout, H., S. Buono, S. Guo, C. Kretz, N. Messaddeq, S. Booten, S. Greenlee, B. P. Monia, B. S. Cowling and J. Laporte (2017). "Antisense oligonucleotide-mediated Dnm2 knockdown prevents and reverts myotubular myopathy in mice." Nat Commun **8**: 15661.

Annex 1: Standard Operating Procedure for Disease Severity Score

STANDARD OPERATING PROTOCOL (SOP)	
Title :	Disease Severity Score (DSS)

This SOP describes the disease severity scoring (DSS) system, based on the original (DSS) published in Tasfaout, Buono et al 2017, and subsequently optimized in Buono et al (associated manuscript).

Objective

The goal of this SOP is to detail the procedure of allocating a disease severity score (DSS) in mice. The DSS is a parameter which is used for the evaluation of the disease severity of the myopathic phenotype in *Mtm1*$^{-/y}$ mice. The calculation is based on 4 parameters: difference of body weight, hanging test ability, kyphosis and walking difficulties. The minimal score is 0 (no myopathic phenotype) and the maximal score is 5 (characterizing a very severe myopathic phenotype).

1. Abbreviations and Definitions

DSS	Disease Severity Score
NHS	Natural History Study
SOP	Standard Operating Protocol
NA	Not applicable

2. Risk Assessment / Related documents

3. Ethics

Mice should be handled according to national legislation on animal care and experimentation. This SOP is in alignment with the French and European legislation. Procedures and Protocols should be approved by the institutional Ethics Committee.

4. Materials and Equipment

- Type 3 cage: 425 x 265 x 150 mm
- Metal Grid : 410 x 270 mm
- Timer
- Scale
- Lid of transport box (optional)

5. Reagents

NA

6. Protocol

1) Body weight

Measure body weight, to 2 decimal places. The score for this parameter (score between 0 and 1) is the difference of a *Mtm1*$^{-/y}$ mouse body weight from week n to n+1:

Table 1: Body weight to score conversion

Body weight	SCORE
X ≥ 0.25g	0
-0.25g > X > 0.25g	0.5
X ≤ -0.25g	1

X(g) = (body weight week n+1(g)) – (body weight week n(g))

2) Hanging test ability

This test must be done one mouse at a time:

a. Take one type 3 cage and one grid.
b. Place mouse in the middle of the grid
c. Turn the grid upside down. The suspending animal should hold on to the grid in order to avoid falling.
    - Test must be set up at a certain height, around 40 cm, for mouse to not being influenced to jump.
d. Prevent the mouse from turning over to the other side of the grid or at pellets food and bottle place by barring with the hand (without touching the mouse) or by using the lid of a transport box.
e. The latency to fall will be measured three times (60 seconds each) for each mouse, with a minimum interval of 10 minutes between trials.
    - The latency time measurements begin when the mouse is hanging free on the wire and end with the animal falling to the cage underneath the wire or grid.
    - If performing the whole body hanging test for the first time, mouse can fall as soon as grip is turned upside down. If this is the case, the first assay can be considered as familiarization of the mouse with the testing conditions and will not be considered as one of the three assays of the test. Only time (seconds) for the three next trials will be reported in the dedicated table (Table 2).
    - If a mouse falls for any other reason that muscle strength default (eg if a mouse is not willing to do the test, voluntary jump from the grip, or falls because of your hands…), this will not be considered as a trial. This must be recorded in the note section in the dedicated table (Table 2)
    - A mouse should normally explore the grid. If a mouse stays in place and does not explore the grip. This must be recorded in the note section in the dedicated table (Table 2)
f. Time (seconds) when mouse falls should be reported in the dedicated table (Table 2).
    - 60 seconds is the maximum time allowed

Table 2: Data collection table for hanging test

			Hanging time (seconds)			
Mice ID number	**Mice genotype**	**Age (weeks)**	**Test 1**	**Test 2**	**Test 3**	**Note**

Note: Mouse genotype should be blinded until experiment is complete

The score for this parameter (score between 0 and 2) represents the mean hanging time according to the formula: Time (s) > [(60-Time (s))/60s]*2 = value (0-2)

Examples:
1s > (60-1)/60*2=1.97
15s > (60-15)/60*2=1.5
30s > (60-30)/60*2=1
60s > (60-60)/60*2=0

3) Kyphosis

This parameter reflects the curvature of the spine. The score is noted as:

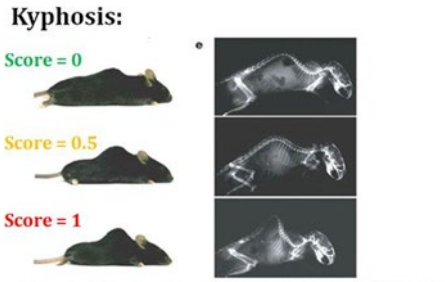

Adapted from Gabellini et *al.* Nature (2006)

Score 0: no curvature of the spine
Score 0.5: mild curvature of the spine
Score 1: severe curvature of the spine

4) Walking difficulties

This parameter reflects the ability to use hindlimbs and the ability of mice for walking. The score is noted as:

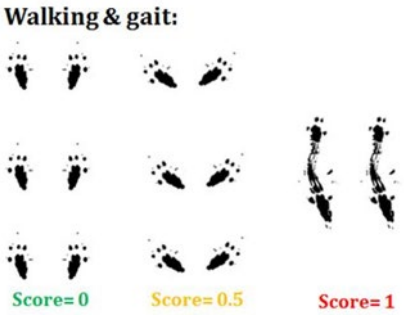

Score 0: normal use of hindlimbs
Score 0.5: splayed use of hindlimbs
Score 1: loss of use of hindlimbs

Note: if score 1:

- indicate if the hindlimbs are paralyzed or not
- indicate if the mouse can still move

7. Calculation of DSS

Disease Severity Score (DSS) is the sum of the scores of the 4 parameters: body weight, hanging test ability, kyphosis and walking difficulties. The maximal DSS is 5.

Note: always refer to ethics application for humane endpoints.

8. Data Collection

All the data concerning the DSS will be reported in the dedicated table (table 3).

Table 3: Data collection table for Disease Severity Score

Mice ID	Mice genotype	Age (weeks)	Body weight	Score body weight	Score hanging	Score walking	Score kyphosis	TOTAL DSS

Note: Mouse genotype should be blinded until experiment is complete

9. Data Analysis

The data will be expressed as a sum of the 4 different parameters: body weight, hanging test ability, kyphosis and walking difficulties

Table 4. Disease severity score (DSS). Tabular summary of DSS procedure, based on natural history study data analysis and modeling from training and test cohorts of *Mtm1*$^{-/y}$ mice (Buono et al, associated manuscript).

Disease severity score	*DSS Description*	*Score*
Body weight	Score 0-1 Difference in body weight between *Mtm1*$^{-/y}$ mouse from week n to n+1.	Score 0: x ≥ 0.25g Score 0.5: -0.25 > x > 0.25 Score 1: x ≤ -0.25g With x being the weight difference
Hanging time	Score of 0-2, representing 0-60 seconds hanging time.	Time (secs) > [(60-Time (s))/60s]*2 = value (0-2) Examples: 1s > (60-1)/60*2=1.967 15s > (60-15)/60*2=1.5 30s > (60-30)/60*2=1 60s > (60-60)/60*2=0
Kyphosis	Score 0-1 Curvature of the spine	Score 0: no curvature of the spine Score 0.5: mild curvature of the spine Score 1: severe curvature of the spine 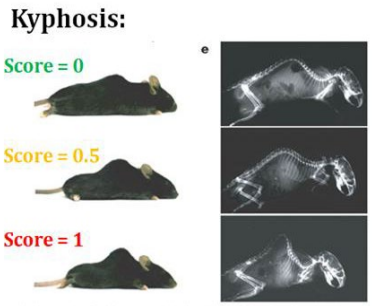 Adapted from Gabellini et *al.* Nature (2006)
Walking difficulties	Score 0-1 Ability to use hindlimbs	Score 0: normal use of hindlimbs Score 0.5: splayed use of hindlimbs Score 1: loss of use of hindlimbs 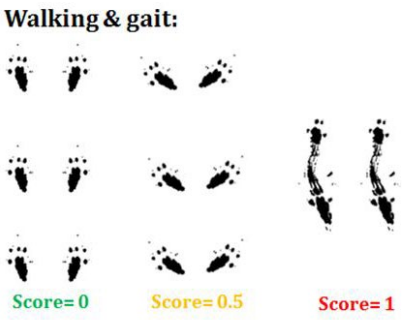
Maximum score	5	